



AIAA 94-3276

**A NUMERICAL STUDY OF DROPLET-VORTEX
INTERACTIONS IN AN EVAPORATING SPRAY**

T. W. PARK and S. K. AGGARWAL
University of Illinois at Chicago
Chicago, IL

&

V. R. KATTA
System Research Laboratory, Inc.
Dayton, OH

DISTRIBUTION STATEMENT A

Approved for public release;
Distribution Unlimited

1/2000 QUALITY INSPECTED 4

19960924 180

**30th AIAA/ASME/SAE/ASEE Joint
Propulsion Conference**
June 27-29, 1994 / Indianapolis, IN

A NUMERICAL STUDY OF DROPLET-VORTEX INTERACTIONS IN AN EVAPORATING SPRAY

T. W. PARK* and S. K. AGGARWAL**

*Department of Mechanical Engineering
University of Illinois at Chicago, Chicago, IL 60607*

and

V. R. KATTA†

*System Research Laboratory, Inc.
Dayton, OH 45440*

ABSTRACT

In this paper, we present the time-dependent axisymmetric numerical simulation of an unsteady n-heptane evaporating spray, and investigate the droplet-vortex interactions which determine the structural and dynamic characteristics of a spray jet flow. The spray is formed between a droplet-laden heated nitrogen jet and a coflowing air stream. A detailed, multidimensional, two-phase algorithm is developed for the simulation. A comprehensive vaporization model is employed to calculate the instantaneous droplet size and surface temperature along the trajectory of each droplet group. Monodisperse spray is introduced into the large vortex structures that are generated due to the presence of buoyancy-induced hydrodynamic instability of the heated jet. Results focused on the two-way interactions between vortical structures and droplets, and the dynamics of both non-evaporating and evaporating sprays. The vortex structures cause droplets to disperse radially outward, and this in turn determines the fuel vapor distribution and also modifies the vortex dynamics. Thus, the dynamics and structural characteristics of the evaporating spray are strongly influenced by the two-way transient interactions. The effects of initial droplet size, injection location, and liquid-to-gas mass loading ratio on these interactions are also investigated.

INTRODUCTION

Large-scale, coherent vortical structures have been found to exist in a variety of shear flows including those involving combustion and multiple phases [1-5]. In two-phase shear flows involving solid particles or liquid droplets, transient interactions between the dispersed phase and the large vortical structures are expected to play a central role in determining the dynamics and structural

characteristics of these flows. The transient interactions pertain to the effect of large vortical structures on the behavior of droplets/particles, and the influence of droplets on the dynamics of large vortical structures. These two effects are coupled in a nonlinear manner; the vortex structures determine the droplet dispersion and gasification behavior, which in turn affects the local environment surrounding each droplet and thereby the dynamics of two-phase system under consideration. Several numerical [6,7] and experimental [8-11] studies in recent years have focused on the one-way coupling, examining the influence of large vortical structures on the dynamics of droplets/particles injected into a shear flow. These studies show that the effect of large structures on particle motion is characterized by the ratio of the particle response time to the characteristic time of structures. This ratio is defined as the Stokes number (St). When the particle response time is of the same order of magnitude as the vortex time scale, $St \sim O(1)$, particles can disperse significantly more than the fluid particles, the enhanced dispersion being attributed to the centrifugal action of vortices. For small Stokes number, $St \ll 1.0$, particles behave similar to the fluid particles, while for large Stokes number, particles remain largely unaffected by the vortices. More recent work [12,13] on particle-laden flows have examined the effect of external forcing on the particle dispersion behavior. A general conclusion from those studies [12,13] is that the dynamics of vortex structures, and thereby the dispersion behavior of particles in a shear layer can be manipulated by a sub harmonic periodic forcing of the shear layer.

Particle-laden shear flows in practical applications involve two-way, nonlinear interactions between the continuous phase and the dispersed phase. Previous studies cited above have mostly focused on the one-way interactions, i.e. on characterizing the effect of vortex structures on the droplet motion and dispersion behavior. The effects of dispersed phase on the vortex dynamics, and subsequently on fuel vapor distribution and flame behavior remain largely unexplored. In this paper, we report a numerical study of two-way droplet-vortex interactions in an unsteady evaporating spray. The spray is formed

* Graduate Student, AIAA Student Member

** Associate Professor, Associate Fellow, AIAA

† Senior Engineer, AIAA Member

between a droplet-laden heated nitrogen jet and a coflowing air stream. The jet velocity and temperature are considered in a range where the large vortical structures are generated due to the buoyancy-induced hydrodynamic instability rather than the shear-induced Kelvin-Helmholtz instability. The vaporization characteristics of n-heptane fuel spray under the influence of two-way droplet-vortex interactions are investigated. The dynamics of a non-evaporating spray is also analyzed in order to distinguish the interactions involving only momentum transfer between the phases from those involving mass, momentum, and energy transfer.

PHYSICAL MODEL

The evaporating spray investigated in the present study is shown schematically in Fig. 1. It consists of a central fuel jet which is a two-phase mixture of gaseous nitrogen and liquid fuel droplets and a low-speed coannulus air flow. The central jet is heated primarily to enhance the fuel evaporation; however, in the present studies, it also plays a key role for the formation of buoyancy induced vortical structures. Numerical studies on the two-way interactions between the vortex structures and the evaporating droplets are conducted by solving the unsteady, axisymmetric gas-phase equations that include the droplet source terms, and the appropriate droplet equations.

The unsteady, axisymmetric governing equations in cylindrical (z, r) coordinate system for heated jet are

$$\begin{aligned} \frac{\partial(\rho\Phi)}{\partial t} + \frac{\partial(\rho u\Phi)}{\partial z} + \frac{\partial(\rho v\Phi)}{\partial r} &= \frac{\partial}{\partial z}(\Gamma^\Phi \frac{\partial\Phi}{\partial z}) \\ &+ \frac{\partial}{\partial r}(\Gamma^\Phi \frac{\partial\Phi}{\partial r}) - \frac{\rho v\Phi}{r} + \frac{\Gamma^\Phi}{r} \frac{\partial\Phi}{\partial r} + S_g^\Phi + S_t^\Phi. \end{aligned} \quad (1)$$

The general form of Eq. (1) represents the continuity, momentum, species, or energy conservation equation depending on the variable used for Φ . Table 1 gives the transport coefficients Γ^Φ and the source terms S_g^Φ and S_t^Φ that appear in the governing equations. In this table, μ , λ , and c_p represent the viscosity, the thermal conductivity, and the specific heat, respectively. They are considered functions of temperature and species concentration.

In order to evaluate the source terms in the gas-phase equations due to the presence of droplets, it is necessary to establish droplet trajectories, size and temperature histories. The Lagrangian approach is employed to solve the liquid-phase governing equations for the dynamics and vaporization history of each droplet group. The spray is characterized by a discrete number of droplet groups, distinguished by their injection location, initial size, and time of injection. The effect of dispersed phase is incorporated through the source/sink terms, representing the exchange of mass, momentum, and energy between the gas and liquid phases. The equations governing the variation of position, velocity, and size for each droplet group and other expressions are available in

Ref. [14]. A comprehensive vaporization model is employed to calculate the instantaneous droplet size and surface temperature along the trajectory of each group. The model includes the effects of variable thermophysical properties, non-unity Lewis number in the gas film outside the droplet, the effect of Stefan flow on the heat and mass transfer between the droplet and the gas, and the effect of transient liquid heating. The variable thermophysical properties are calculated at reference film temperature and concentrations, obtained by using the 1/3 rule, except for the gas density which is calculated at the free stream value [15]. The Wilke rule [16] is used to calculate the dynamic viscosity and thermal conductivity of the gas film. The droplet (nC_7H_{16}) properties are collected from the various sources and approximated as a function of the temperature [14]. The effect of transient liquid heating is incorporated by using the conduction-limit model [17]. This model is deemed satisfactory in the present study, since the maximum droplet Reynolds number during droplet lifetime is less than ten and thus the effect of internal circulation is expected to be negligible. For the same reason, the effects of gas-phase convection on the heat and mass transport are represented by the Ranz-Marshall correlation [17].

SOLUTION PROCEDURE

The numerical solution of the unsteady two-phase equations employs an implicit algorithm for solving the gas-phase equations, and an explicit Runge-Kutta procedure for the liquid-phase equations. The finite-difference forms of the momentum equations are obtained using an implicit QUICKST scheme [18], while those of the species and energy equations are obtained using an hybrid scheme of Spalding [19]. A "finite control volume" approach with a staggered, non-uniform grid system is utilized. Body force term due to gravitational field is included in the axial momentum equation for gas-phase and the droplet motion equation for liquid-phase. An iterative ADI (Alternative Direction Implicit) technique is used for solving the resulting sets of algebraic equations. A stable numerical integration procedure is achieved by coupling the species and energy equations through the source terms (cf. Table. 1). At every time step, the pressure field is calculated by solving the pressure Poisson equations simultaneously and utilizing the LU (Lower and Upper diagonal) matrix decomposition technique. It should be noted that the pressure Poisson equations consider the effect of mass transfer from the liquid phase to the gas phase, represented by a source term in the gas-phase mass continuity equation.

The liquid-phase equations are advanced in time by a second-order accurate Runge-Kutta method. Since the gas-phase solution employs an implicit procedure, the temporal step size used for integrating the liquid-phase equations is smaller than that for gas-phase equations. An automatic procedure is implemented in order to select an optimum liquid-phase time step. The procedure involves calculating the characteristic thermal response time,

velocity response time, and vaporization time for each droplet group, and then selecting the temporal step size as a fraction (two-hundredth) of the smallest of these time scales. A detailed examination of the various time scales, based on numerical experiments, revealed that the temporal step size is determined by either the thermal response time or the velocity response time of a given droplet group. The number of sub cycles for advancing the liquid-phase solution for each gas-phase cycle typically varies from two to ten, depending upon the droplet size.

The procedure to advance the two-phase solution over one gas-phase time step is as follows. Using the known gas-phase properties, the liquid-phase equations are solved over a specified number of liquid-phase subcycles. A third-order accurate Lagrangian polynomial method is used for interpolating the gas-phase properties from the non-uniform fixed grid to the droplet characteristic location. It should be noted that the interpolation scheme for the gas-phase velocities u and v is based on their respective grid cells because of the use of a staggered grid in gas-phase calculation. The droplet properties are updated after every liquid-phase subcycle. Also, during each subcycle, the liquid-phase source terms appearing in the gas-phase equations are calculated at the characteristic location, and then distributed to the surrounding gas-phase grid points. These source terms are added at each gas-phase grid points during one gas-phase time step and then used in the implicit solution of the gas-phase equations.

RESULTS

The jet diameter of the vertically mounted evaporating spray considered in the present study is 2.54 cm. The jet velocities for the central fuel and coannular air streams are 1.0 and 0.2 m/s, respectively. Flat velocity profiles are used as the inflow conditions. Temperature chosen for the fuel jet is 1200 K while that of the surrounding annulus air is 294 K. Calculations are made for a physical domain having dimensions of 15 and 40 cm in the radial and axial direction, respectively. It should be noted that the physical domain used in the calculations is much larger than the domain of interest (3 x 20 cm) and hence, the results are not influenced by the computational boundaries.

Results reported in the present paper are obtained using a grid system having 151 and 61 points in the axial and radial directions, respectively. Calculations are advanced in time utilizing a low CFL number of 0.2. In an earlier study of gas-phase simulations [14] it was found that the results obtained on a 151X61 grid system and using a CFL number of < 0.5 are grid independent and time accurate.

Calculations are initially made without injecting droplets into the fuel stream. The shear layer between the 1200 K-nitrogen jet and the cold annulus air flow became unsteady with the development of large-scale vortices. Iso-temperature contours of this heated jet are shown in

Fig. 2(a). It is important to note that these vortical structures are generated without using any external forcing, and their dynamics is found to be highly periodic. The numerical experiments [14] have indicated that the large-scale toroidal vortices appear as a result of the buoyancy-induced instability of the heated-jet shear layer. In other words, the buoyant acceleration of the hot gases in the shear layer is primarily responsible for this instability.

Numerical experiments are conducted by injecting different groups of droplets into the fuel stream to examine the changes in the flow structure due to the two-way nonlinear, two-phase interactions. The injection process consists of introducing a group of monodisperse droplets at a given instant of time. The number of droplets in each group depends on the mass loading (mass ratio between the liquid fuel and the nitrogen gas), initial droplet size, and injection time interval. As a base case for the spray calculations reported in this work, a monodisperse n-heptane spray with an initial diameter of 200 μm and mass loading of 1 is considered. The droplets are injected continuously into the jet shear layer from a radial location of 1.25 cm. A time difference of 1.428 ms is used between two consecutive injections for all the spray calculations reported in this work. This time interval was determined based on the constraint that the spatial separation between two successive droplet groups is large enough for neglecting the interaction between the droplets. This yields the number of droplets in each group to be 76.

The instantaneous iso-temperature contours for the base spray case are shown in Fig. 2(b). All the droplet source terms (cf Table 1) are incorporated in the gas-phase equations. No effort is made in matching the phases of the gaseous and spray jets of Fig. 2. It is apparent from this figure that the injection of 200 μm droplets into the shear layer weakened the vortical structures and decreased the spreading of the heated jet. The latter is as expected due to the fact that the addition of fuel spray to the nitrogen gas increases the jet momentum. On the other hand, the reason for the former effect (i.e., weakening of vortices) is not clear. However, it may be attributed to the non-linear coupling of two-phase flow.

The dynamics of the vortex structures is examined by plotting time evolution of temperature contours in Fig. 3. Temperature data along the radial location at an axial location of 10 cm above the jet exit for the gaseous and spray cases are recorded over a time period of 240 ms and shown in this figure. It can be seen from Fig. 3(a) that the vortex structures in the case of gaseous jet are highly coherent and periodic. The frequency of oscillation is 15.8 Hz. With the addition of fuel spray the dynamics of jet has become aperiodic and also the vortex crossing frequency has increased by about 30 % (from 15.8 to 20.5 Hz).

Effect of Liquid Mass Loading

The structural changes noted in a buoyancy driven heated jet with the addition of fuel spray are resulting from 1) liquid mass loading, 2) droplet evaporation, and 3) the two-way interaction between the vortices and the droplets. To further understand the impact of the above individual parameters, numerical experiments are made by changing the liquid mass loading, evaporation characteristics, spray injection location and the droplet size.

1. Non-Evaporating Spray

The instantaneous iso-temperature contours for five different mass loading values ($M = 0, 0.125, 0.25, 0.50$, and 1.0) for a non-evaporating spray case are shown in Fig. 4. Here, the mass loading M is defined as the ratio between the mass flow rate of the liquid droplets and that of the nitrogen gas. Liquid mass flow rate is controlled by changing the number of droplets in each injected group. As the droplets are assumed to be non-evaporating ones in this case, only the source terms in the momentum equation (cf Table 1) are considered in gas-phase equations. In other words, only the momentums are exchanged in this two-phase flow calculations. The single-phase gaseous flow shown in Fig. 2(a) may be approximated as a non-evaporating spray in the limiting case of $M = 0$ [Fig. 4(a)]. It seems that the structural characteristics of low mass loading cases like $M = 0.125$ and 0.25 are similar to that of single-phase flow even though the vortex-crossing frequencies in these flows are somewhat different.

The time history plots of the dynamic heated jets for different mass loading values are shown in Fig. 5. This plot clearly shows the changes in the sizes of the vortex structures and their crossing frequency for different cases. It may be observed from Fig. 5 that as the mass loading ratio is increased, the crossing frequency of vortex structures is also increasing. At higher mass loading values ($M = 0.5$ and 1.0), the structural characteristics seem to change more significantly.

2. Evaporating Spray

The effect of mass loading in an evaporating spray is depicted by plotting the instantaneous temperature contours for several mass loading values ($M = 0.25, 0.5$ and 1.0) in Figure 6. The gas-phase governing equations for this case include all the source/sink terms due to the exchange of mass, momentum and energy due to droplets dynamics and vaporization. Structure of the heated jet seems to change more significantly with the addition of evaporating spray compared to that of a non-evaporating one.

Figure 7 shows the time evolution of temperature contours at $z = 7.5$ cm for the three cases shown in Fig. 6. It is interesting to compare the structures of high mass loading values ($M = 0.5$ & 1.0) for the evaporating (Fig.

7) and non-evaporating (Fig. 5) cases. The development of vortical structures for evaporating spray is more periodic than that observed in the corresponding non-evaporating cases.

Effect of Injection Location

The effect of initial droplet distribution on the structural characteristics and dynamics of the heated spray jet is studied by changing the injection locations. The mass loading ratio and the size of the droplet are fixed at 1.0 and $200 \mu\text{m}$, respectively. Evaporating spray jets are simulated in this study. The instantaneous temperature contours for three cases having different droplet injection locations are shown in Fig. 8. The three distributions of injection locations used are as follows; 1) $r_k = 1.25$ cm, 2) $r_k = 0.625$ and 1.25 cm, and 3) $r_k = 0.25, 0.50, 0.75, 1.00$ and 1.25 cm. The mass loading ratio is kept constant by using different number of droplets in each group for different cases. It is shown that the characteristics of core region near nozzle exit are quite different for all the three cases due to different initial droplet injection process. The use of more injection locations apparently led to a dynamic heated spray jet with well-organized vortical structures [Fig. 8(c)]. It is known that the vaporization of liquid droplet absorbs thermal energy and hence reduces the local temperature. This is evident in Figs. 8(b) and 8(c). In the former figure a valley in the temperature contours developed in the downstream region of the inner injection location (i.e., $r_k = 0.625$ cm) as the injected droplet vaporizes. However, in the latter figure, the choice of more injection locations reduced the entire jet temperature uniformly leading to near flat contours for 1000 and 1100 K [Nos. 7 and 8 in Fig. 8(c)].

The time evolution for temperature contours at an axial location of 7.5 cm for the three cases of injection locations are plotted in Fig. 9. It clearly shows that the vortex structures are well organized and highly periodic similar to that of a single-phase flow [Fig. 2(a)] when the number of injection locations is large.

Effect of Droplet Size

The instantaneous temperature contours represented in Figs. 10(a), 10(b), and 10(c) show the structures of three different n-heptane evaporating sprays with initial droplet diameters (d_0) of $50, 100$, and $200 \mu\text{m}$, respectively. A constant mass loading ratio of $M = 1.0$ is obtained for different cases by increasing the number of droplets in each group as its initial size is decreased. Droplets in all the three cases are injected in the shear layer ($r_k = 1.25$ cm). The important observation made from these calculations is that the initial droplet size has a strong influence on the structural characteristics of the evaporating sprays. Vortex structures of the $50\text{-}\mu\text{m}$ evaporating spray [Fig. 10(a)] seem to be destroyed in the downstream of $z = 10$ cm.

Reduction of temperature due to vaporization of the liquid fuel is evident in these calculations made with different initial droplet sizes. In fact, when the droplet size is very small ($\sim 50 \mu\text{m}$) the temperature of the entire fuel/ N_2 jet downstream of $z = 100 \text{ cm}$ has dropped down to less than 400 K from the initial temperature of 1200 K. The time evolution of temperature contours for the three evaporating sprays with different initial droplet sizes are shown in Fig. 11. The structural dynamics is very different for all the three cases. Due to subsequent vortex pairing phenomena between the axial locations $z = 2.5$ and 5 cm (not shown in the figures), the structures of 50- μm case became large and their crossing frequency has decreased. It seems that the two-way nonlinear interactions became stronger due to the high concentrated fuel vapor in a jet shear layer region by fast vaporization of 50- μm evaporating spray.

CONCLUSIONS

In this paper, the droplet/vortex interactions on the dynamics of evaporating spray and their structural characteristics are studied by developing a detailed multidimensional numerical algorithm. An implicit, third-order accurate QUICKEST scheme for momentum equations and hybrid scheme of Spalding for species and energy equations are used to solve the unsteady axisymmetric gas-phase equations. The Lagrangian approach is employed to study the droplet dynamics and vaporization history in an evaporating spray. The effect of dispersed phase is incorporated through the source/sink terms in the gas-phase governing equations, representing the exchange of mass, momentum, and energy between the gas and liquid phases.

Snapshots and time evolution plots of temperature contours are employed to analyze the structural characteristics and their dynamics of the non-evaporating and evaporating spray jet flow. The presence of gravity introduces the buoyancy-induced hydrodynamic instability, causing the large vortical structures to appear without any external perturbation. The vortex structures cause droplets to disperse radially outward, and this in turn determines the fuel vapor distribution and also modifies the vortex dynamics. Thus, the dynamics and structural characteristics of the evaporating spray are strongly influenced by these interactions. The effects of initial droplet size, injection location, and liquid-to-gas mass loading ratio on the droplet/vortex interaction are also investigated by performing numerical experiments.

The important observations made from this study are: (1) A strong two-way nonlinear, two-phase interaction between large vortex structures and droplets is observed in non-evaporating and evaporating sprays. (2) The structural characteristics and their dynamics for both non-evaporating and evaporating spray are significantly affected at high liquid-to-gas mass loading ratios ($M \geq 0.5$). (3) The vortex structures become highly coherent and periodic as the multiple injection locations are chosen

for the high liquid-to-gas mass loading case ($M = 1.0$). (4) The initial droplet size has a strong effect on the structural characteristics and their dynamics. Also, the subsequent vortex pairing phenomena is observed for the 50- μm evaporating spray.

ACKNOWLEDGMENT

This work was supported by AFOSR Grant F49620-92-J-0231, with Dr. Julian M. Tishkoff as the Program Manager. Many fruitful discussions with Dr. W. M. Roquemore at Wright-Patterson Air Force Base are greatly appreciated.

REFERENCES

1. Brown, G. L., Roshko, A., "Density Effects and Large Scales in the Developing Mixing Layer," *J. Fluid Mech.*, Vol. 64, pp. 775-816, 1974.
2. Yule, A. J., "Large Scale Structure in the Mixing Layer of a Round Jet," *J. Fluid Mech.*, Vol. 89, pp. 413-432, 1978.
3. Katta, V. R., Goss, L. P., and Roquemore, W. M., "Effect of Nonunity Lewis Number and Finite-Rate Chemistry on the Dynamics of a Hydrogen-Air Jet Diffusion Flame," *Combustion and Flame*, Vol. 96, pp. 60-74, 1994.
4. Longmire, E. K. and Eaton, J. K., "Structure of a Particle-Laden Round Jet," *J. Fluid Mech.*, Vol. 236, pp. 217-257, 1992.
5. Park, T. W., Aggarwal, S. K., and Katta, V. R., "Effect of Gravity on the Structure of an Unsteady Spray Diffusion Flame," to appear in *Combustion and Flame of the Twenty-Fifth Symposium (International) on Combustion*, 1994.
6. Chung, J. N., and Troutt, T. R., "Simulation of Particle Dispersion in an Axisymmetric Jet," *Journal of Fluid Mechanics*, Vol. 186, pp. 199-222, 1988.
7. Hansell, D., Kennedy I. M., and Kollmann, W., "A Simulation of Particle Dispersion in a Turbulent Jet," *International Journal of Multiphase Flow*, Vol. 18, No. 4, pp. 559-576 1992.
8. Lazaro, B. J., and Lasheras, J. C., "Particle Dispersion in the Developing Free Shear Layer, Part 1- Unforced Flow," *Journal of Fluid Mechanics*, Vol. 235, pp. 143- 178, 1992.
9. Lazaro, B. J., and Lasheras, J. C., "Particle Dispersion in the Developing Free Shear Layer, Part 2- Forced Flow," *Journal of Fluid Mechanics*, Vol. 235, pp. 179- 221, 1992.
10. Samimy, M., and Lele, S. K., "Motion of Particles with Inertia in a Compressible Free Layer," *Physics of Fluids*, Vol. A 3, pp. 1915-1923, 1991.
11. Hishida K., Ando, A., and Maeda, M., "Experiments on Particle Dispersion in a Turbulent Mixing Layer," *International Journal of Multiphase Flow*, Vol. 18, pp. 181-194, 1992.
12. Uthuppan, J., Aggarwal, S. K., Grinstein, F. F., and Kailasanath, K., "Particle Dispersion in a Transitional Axisymmetric Jet : A Numerical

- Simulation," AIAA 93-0105, 31st Aerospace Sciences Meeting and Exhibit, Reno, Nevada, 1993. Also to appear in AIAA Journal.
13. Aggarwal, S. K., "Relationship Between Stokes Number and Intrinsic Frequencies in Particle Laden Flows," AIAA Journal, Vol. 32, No. 6, pp. 1322-1325, 1994.
 14. Park, T. W., Aggarwal, S. K., and Katta, V. R., "Gravity Effects on the Dynamics of Evaporating Droplets in a Heated Jet," AIAA Paper 94-0684, 32nd Aerospace Sciences Meeting and Exhibit, Reno, 1994. Also submitted to AIAA J. of Propulsion and Power.
 15. Abramzon, B. and Sirignano, W. A., Int. J. Heat Mass Transfer, 32 (9): 1605-1618 (1989).
 16. Edwards, D. K., Denny, V. E. and Mills, A. F., Transfer Processes: An Introduction to Diffusion, Convection and Radiation (2nd Edn.), McGraw-Hill, New York, 1979.
 17. Aggarwal, S. K., Tong, A. and Sirignano, W. A., "A Comparison of Vaporization Models for Spray Calculation," AIAA Journal, Vol. 22, No. 10, pp. 1448-1457, 1984.
 18. Leonard, B. P., A Stable and Accurate Convective Modeling Procedure Based on Quadratic Upstream Interpolation, Comput. Methods in Applied Mechanics and Engineering, Vol. 19, pp. 59-98, 1979.
 19. Spalding, D. B., Int. J. Num. Meth. Eng., Vol. 4, pp. 551-559, 1972.

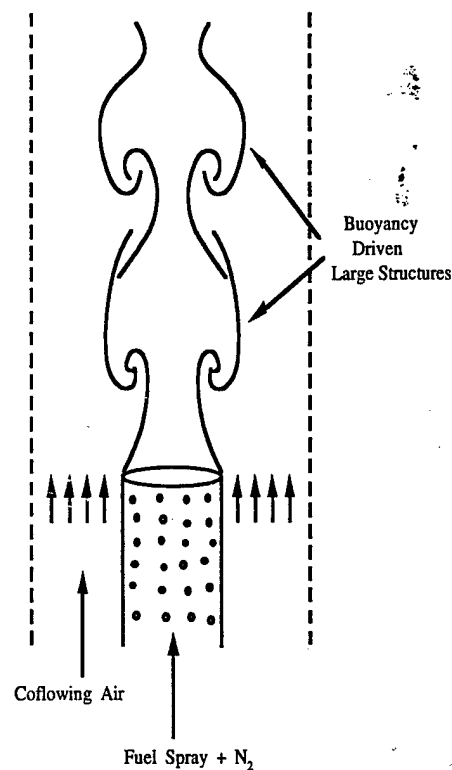


Figure 1: A schematic of evaporating spray jet at 1g.

Table 1: Transport coefficients and source terms appearing in governing equations

Equations	Φ	$\Gamma\Phi$	$S_g\Phi$	$S_l\Phi$
Continuity	1	0	0	$\sum_k n_k \dot{m}_k$
Axial momentum	u	μ	$-\frac{\partial p}{\partial z} + (\rho_0 - \rho)g + \frac{\partial}{\partial z}(\mu \frac{\partial u}{\partial z}) + \frac{\partial}{\partial r}(\mu \frac{\partial v}{\partial z}) + \frac{\mu}{r} \frac{\partial v}{\partial z}$ $-\frac{2}{3} \{ \frac{\partial}{\partial z}(\mu \frac{\partial u}{\partial z}) + \frac{\partial}{\partial z}(\mu \frac{\partial v}{\partial r}) + \frac{\partial}{\partial r}(\mu \frac{v}{r}) \}$	$\sum_k (n_k \dot{m}_k u_k - n_k M_k \frac{du_k}{dt})$
Radial momentum	v	μ	$-\frac{\partial p}{\partial r} + \frac{\partial}{\partial z}(\mu \frac{\partial u}{\partial r}) + \frac{\partial}{\partial r}(\mu \frac{\partial v}{\partial r}) + \frac{\mu}{r} \frac{\partial v}{\partial r} - 2\mu \frac{v}{r^2}$ $-\frac{2}{3} \{ \frac{\partial}{\partial r}(\mu \frac{\partial u}{\partial z}) + \frac{\partial}{\partial r}(\mu \frac{\partial v}{\partial r}) + \frac{\partial}{\partial r}(\mu \frac{v}{r}) \}$	$\sum_k (n_k \dot{m}_k v_k - n_k M_k \frac{dv_k}{dt})$
Mass fraction of fuel	Y_F	ρD	0	$\sum_k n_k \dot{m}_k$
Energy	T	λ/C_p	0	$\sum_k n_k \dot{m}_k (h_{fs} - l_{k,eff})$

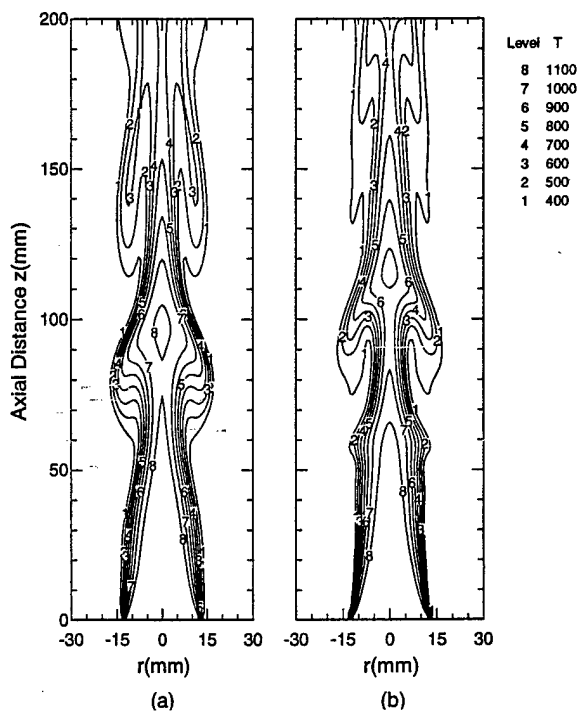


Figure 2: Instantaneous iso-temperature contours for the heated N_2 jet (a) without fuel spray (b) with fuel spray.

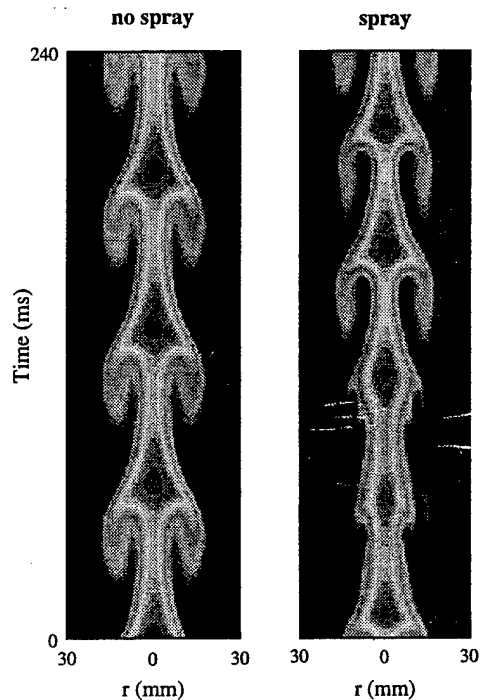


Figure 3: Time evolution of temperature contours at axial location of 10 cm above inlet for the cases of Fig. 2.

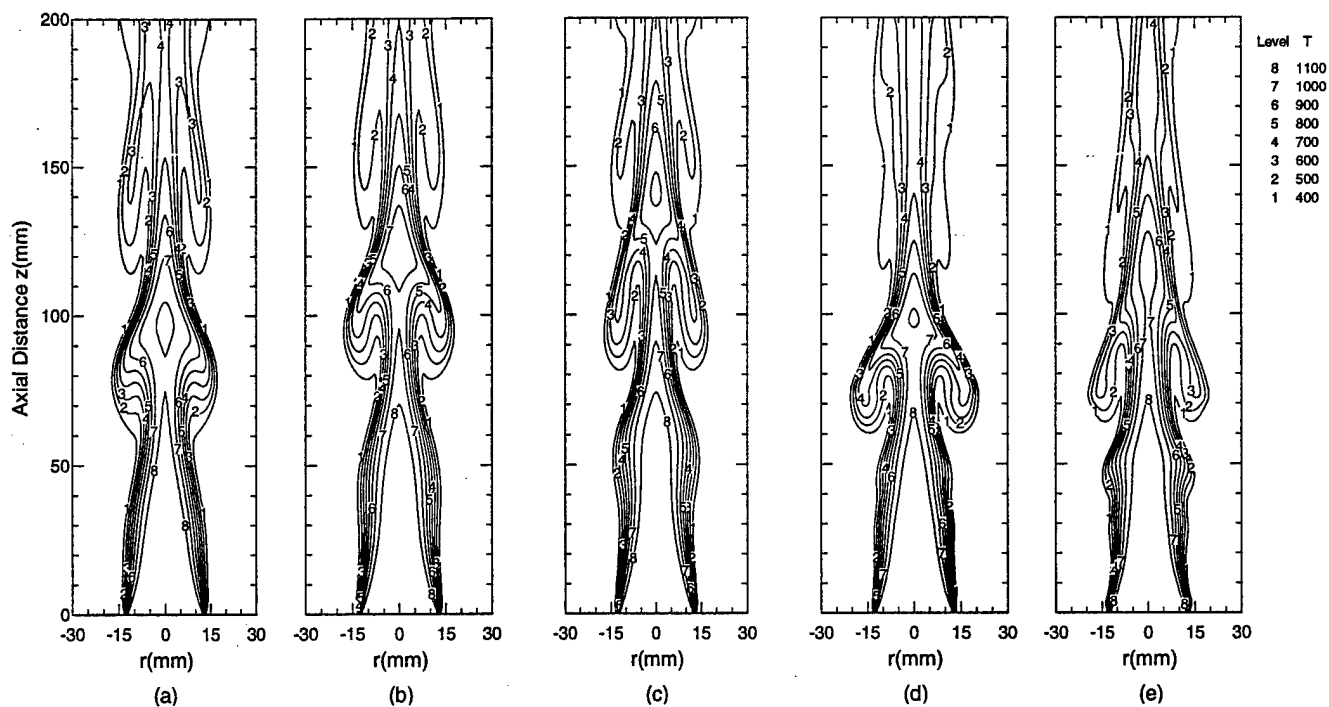


Figure 4: Instantaneous iso-temperature contours for a non-evaporating spray jet with five different mass loading values; (a) $M = 0$, (b) $M = 0.125$, (c) $M = 0.25$, (d) $M = 0.5$, and (e) $M = 1.0$.

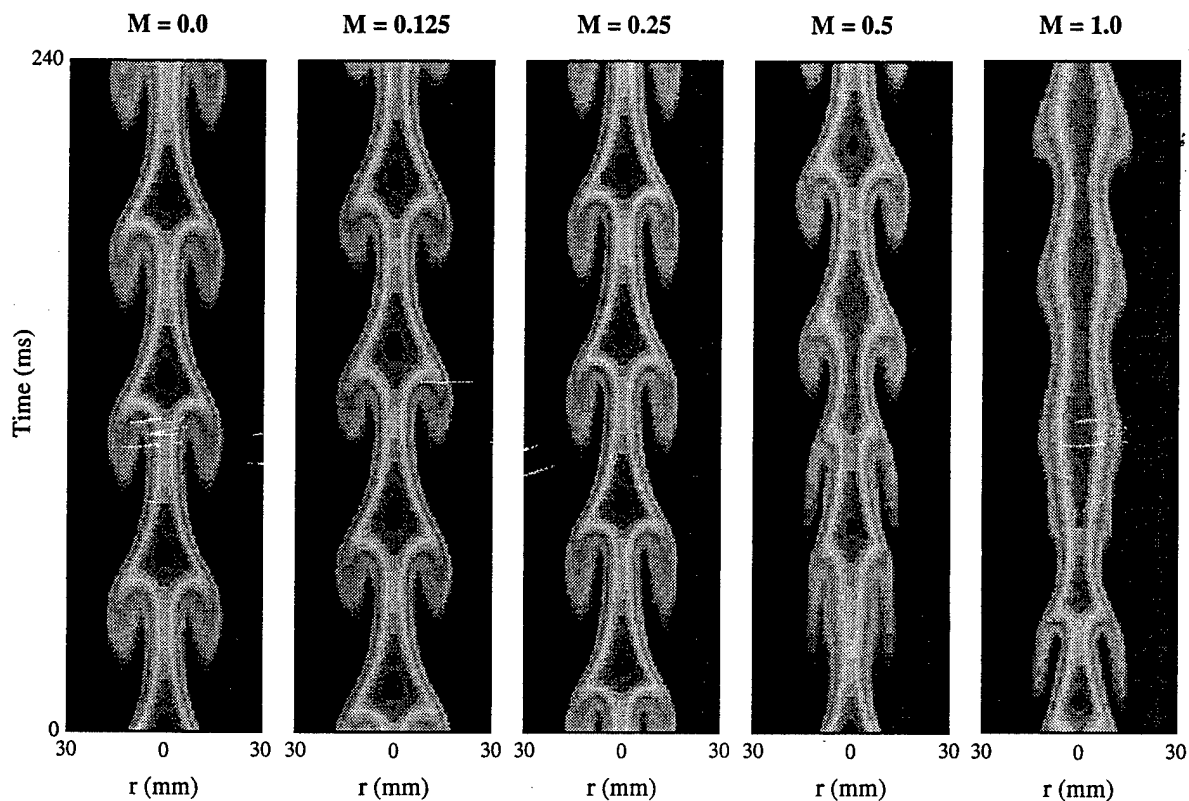


Figure 5: Time evolution of temperature contours at axial location of 10 cm above the inlet for the cases of Fig. 4.

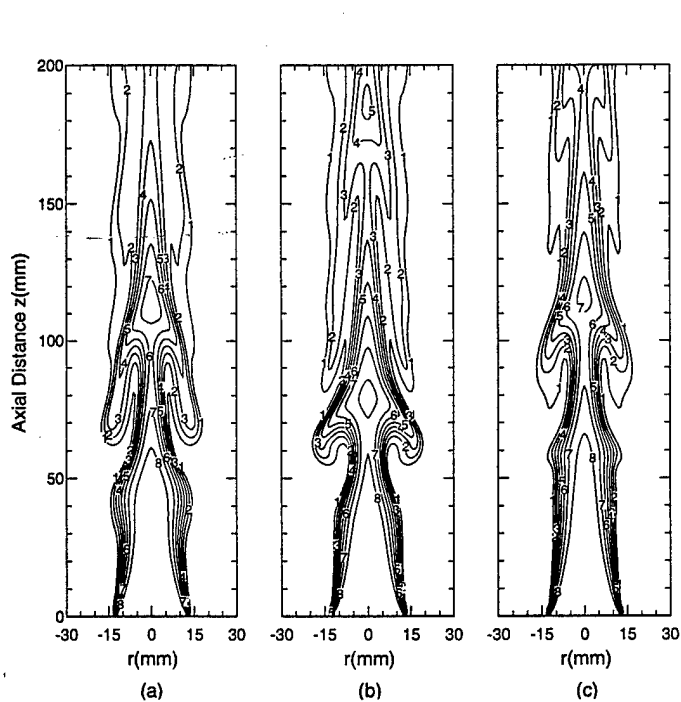


Figure 6: Instantaneous iso-temperature contours for an evaporating spray jet with three different mass loading values; (a) $M = 0.25$, (b) $M = 0.5$, and (c) $M = 1.0$.

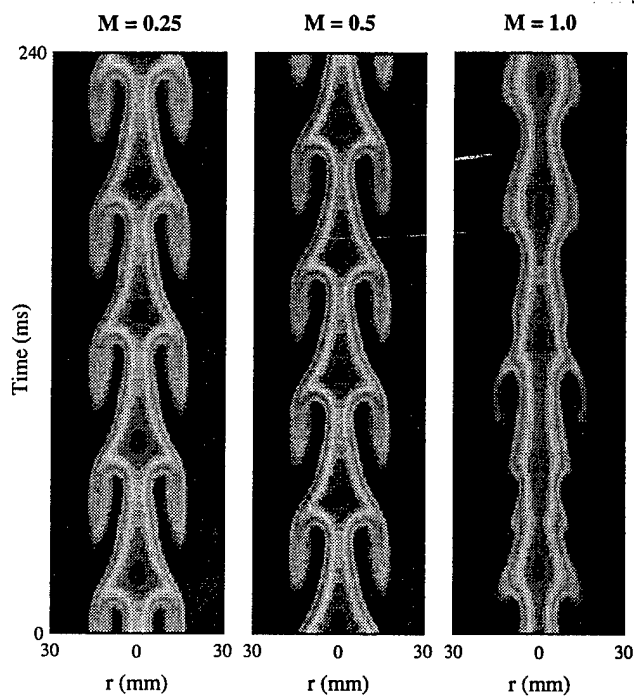


Figure 7: Time evolution of temperature contours at a location of 7.5 cm above the inlet for the cases of Fig. 6.

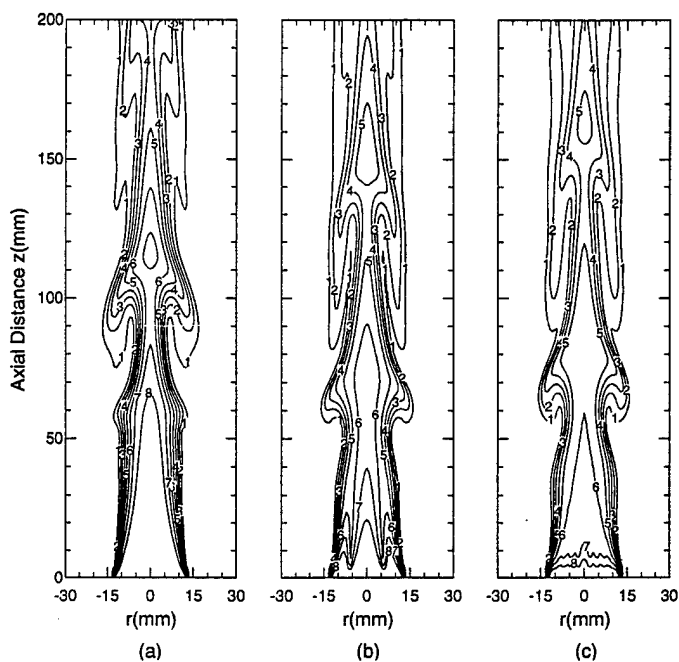


Figure 8: Instantaneous iso-temperature contours for an evaporating spray jet with three different injection distributions; (a) $r_k = 1.25$ cm, (b) $r_k = 0.625$ and 1.25 cm, and (c) $r_k = 0.25, 0.5, 0.75, 1.0$ and 1.25 cm

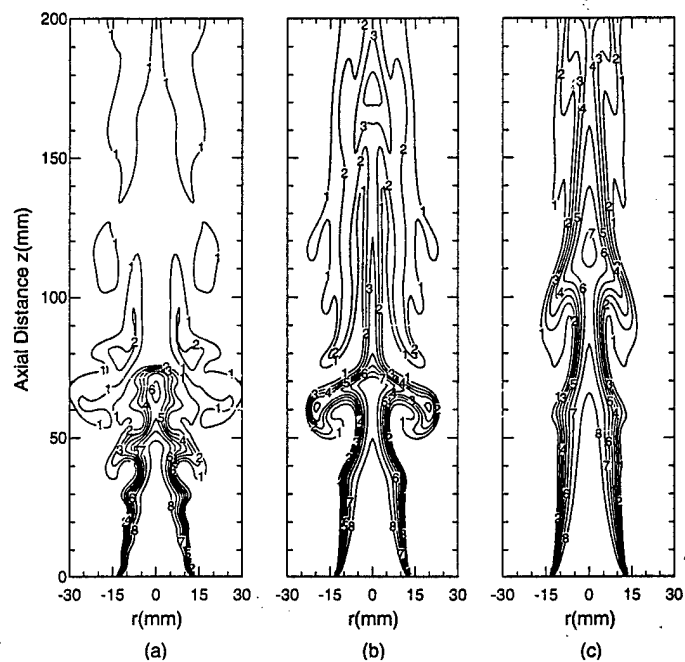


Figure 10: Instantaneous iso-temperature contours for an evaporating spray jet with three different initial droplet diameters; (a) $d_o = 50$ μm , (b) $d_o = 100$ μm , and (c) $d_o = 200$ μm .

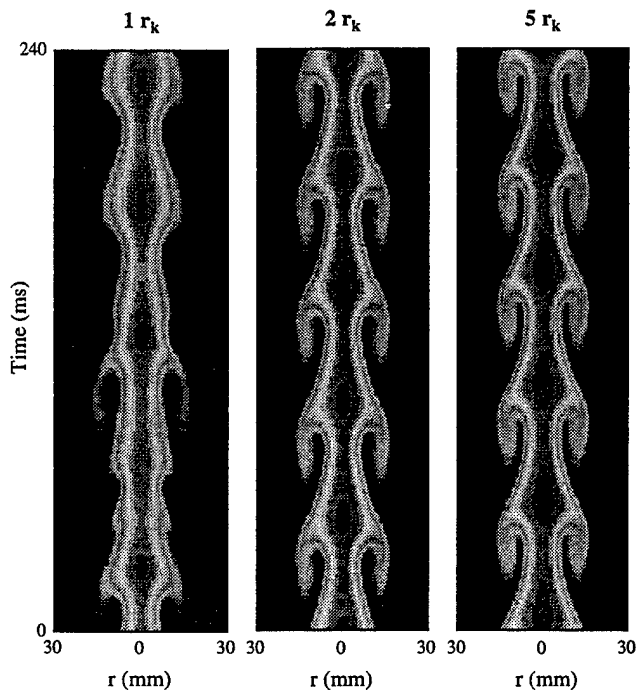


Figure 9: Time evolution of temperature contours at axial location of 7.5 cm above inlet for the cases of Fig. 8.

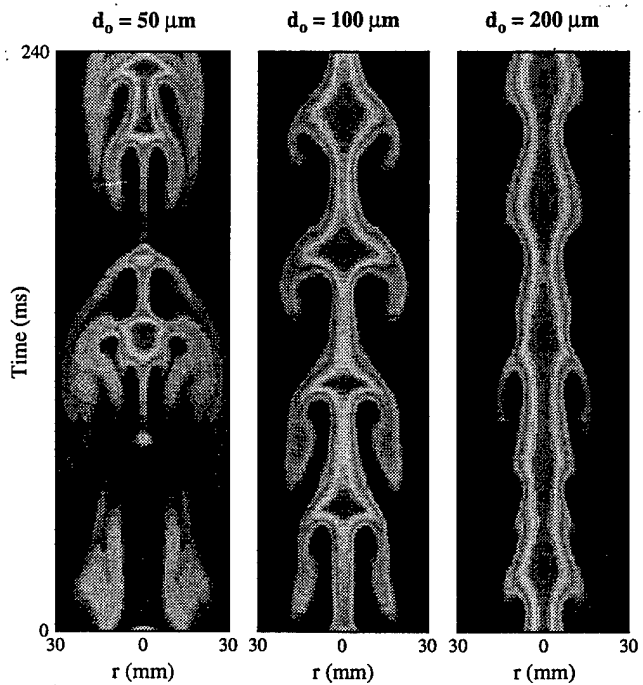


Figure 11: Time evolution of temperature contours at a location 7.5 cm above the inlet for the cases of Fig. 10.